JOURNAL OF GEOPHYSICAL RESEARCH, VOL. 102, NO. B12, PAGES 27,341–27,354, DECEMBER 10, 1997

Variations in axial morphology along the Galápagos spreading center and the influence of the Galápagos hotspot

J. Pablo Canales,[1,2] Juan José Dañobeitia,[1] Robert S. Detrick,[3] Emilie E. E. Hooft,[3] Rafael Bartolomé,[1] and David F. Naar[4]

Abstract. The Galápagos Spreading Center (GSC) is marked by systematic changes in axial morphology between the Inca Fracture Zone (FZ) at 85.5°W and the 95.5°W propagator. We analyze these changes using new swath bathymetry and magnetic data acquired aboard the B/O *Hespérides* during the Galápagos'96 experiment. Within ~350 km of the Galápagos hotspot the ridge axis is associated with an East Pacific Rise (EPR)-like axial high. At increasing distance from the hotspot the axial high broadens and deepens forming a distinctive transitional axial morphology (TAM). The axis in this transitional region is typically a broad zone (~20 km wide) consisting of very rough volcanic and fault-generated topography. West of 95°W, this TAM evolves into a 20-40 km wide, 400-1500 m deep axial valley typical of the slow spreading Mid-Atlantic Ridge (MAR). There is not an abrupt change from axial high to rift valley along the GSC, but a distinct TAM occurs over a distance of ~200-300 km along-axis and is accompanied by a gravity-estimated crustal thickening of >1-2 km. The boundary between an axial high and this TAM is quite abrupt and occurs along a segment that is less than 9 km long. These changes in axial morphology are primarily caused by variations in magma supply along the GSC due to the entrainment and dispersal of plume mantle from the Galápagos hotspot. However, the changes in morphology are not symmetric about the Galápagos FZ at 91°W. The axial high topography extends farther east of the 91°W FZ than to the west, and the rift valley which develops west of 94°W is not found at comparable distances along the GSC east of the hotspot. Axial depth variations are also asymmetric across the 91°W FZ. This asymmetry in both morphology and axial depth variation is attributed to a full spreading rate increase along the GSC from 46 mm/yr at 97°W to 64 mm/yr at 85°W. Off-axis depth changes are symmetric about the 91°W FZ and suggest that 15-40% of on-axis depth variation is dynamically supported.

1. Introduction

The morphology of mid-ocean ridges varies systematically with spreading rate [*Macdonald*, 1982]. Spreading centers with full spreading rates of less than 50 mm/yr, as observed along the Mid-Atlantic Ridge (MAR), typically are associated with 1-2 km deep, 15-30 km wide rift valleys flanked by rough and faulted topography. In contrast, fast spreading ridges (>80 mm/yr full rate), like the East Pacific Rise (EPR), are usually characterized by a 2-10 km wide, 200-400 m axial high flanked by smoother abyssal hill terrain. Intermediate-rate spreading ridges (50-80 mm/yr full rate), like the Southeast Indian Ridge (SEIR), the Juan de Fuca/Gorda Ridges, and the Central Spreading Ridge in the North Fiji Basin often show both axial highs and rift valleys, as well as a transitional morphology intermediate between these two end-members [*Hooft and Detrick*, 1995; *Ma and Cochran*, 1996; *Gràcia et al.*, 1996]. Spreading rate is not, however, the only variable controlling ridge crest morphology. For example, the Reykjanes Ridge is associated with an axial high despite a spreading rate of only 20 mm/yr [*Searle and Laughton*, 1981], while the Australian-Antarctic Discordance (AAD) has an axial valley even though this section of the SEIR is opening at 70 mm/yr [*Sempéré et al.*, 1991].

These observations have led to the view that axial morphology is ultimately controlled by the thermal structure at the ridge axis, which is a function of both spreading rate and magma supply [*Phipps Morgan and Chen*, 1993]. The integrated strength of the lithosphere in the axial region determines how it deforms under extensional stresses and thus controls whether the ridge crest forms an axial high (weak lithosphere which is isostatically compensated) or a rift valley (stronger lithosphere which deforms by brittle-plastic necking) [*Chen and Morgan*, 1990]. *Phipps Morgan and Chen* [1993] have shown how the axial yield strength may be determined by the interplay between hydrothermal circulation and the advection of heat by magma emplacement (which depends on spreading rate and crustal thickness). An increased magma supply at a fixed spreading rate increases the heat supply, creating a thicker crust and a hotter, weaker lithosphere. The *Phipps Morgan and Chen* [1993] model predicts that the transition from an axial valley to an axial high morphology will shift to a slower spreading rate as magma supply (crustal thickness) increases. This particular model also predicts that for a given spreading rate, small changes in crustal thickness produce a rapid change in axial yield strength and thus in axial morphology.

[1]Departamento de Geofísica, Instituto de Ciencias de al Tierra (Consejo Superior de Investigaciones Científicas), Barcelona, Spain.

[2]Now at Department of Geology and Geophysics, Woods Hole Oceanographic Institution, Woods Hole, Massachusetts.

[3]Department of Geology and Geophysics, Woods Hole Oceanographic Instiution, Woods Hole, Massachusetts.

[4]Department of Marine Sciences, University of South Florida, St. Petersburg.

Paper number 97JB01633.
0148-0227/97/97JB-01633$09.00

The nature of the transition between an axial high and an axial valley can thus place important constraints on ridge crest topography models. However, comparatively few studies have been made of this morphological transition. *Small and Sandwell* [1989] analyzed Geosat altimetric-derived gravity data across mid-ocean ridges and showed that there is an abrupt change in the amplitude of the axial gravity anomaly at spreading rates of 60-70 mm/yr. They concluded that ridge-axis morphology is controlled by a threshold phenomenon separating two dynamically distinct modes of seafloor spreading. *Hooft and Detrick* [1995] argued that the major differences in axial morphology between the southern Juan de Fuca Ridge and the Gorda Ridge are associated with quite small differences in crustal thickness (<1 km) and mantle temperature (10-15°C). Thus the transition from rift valley to axial high appears to occur abruptly on a global scale and to be sensitive to small changes in spreading rate or magma supply. Recent studies have described a distinct transitional ridge axis morphology characterized by a shallow (<700 m deep) axial valley [*Cochran et al.*, 1997] or a broad, low-amplitude, rifted axial high [*Gràcia et al.*, 1996; *Cochran et al.*, 1997]. The morphology of the SEIR has recently been extensively analyzed [*Cochran et al.*, 1997; *Ma and Cochran,* 1996, 1997; *Sempéré et al.*, 1997; *Goff et al.*, 1997]. Morphological transitions along this ridge are well-defined and occur over short lengths of the ridge, represent different forms of axial structure, and correlate with changes in mantle Bouguer gravity anomalies and bathymetric roughness.

In this paper we examine the effect of variations in both spreading rate and magma supply on the axial morphology of the Galápagos Spreading Center (GSC). The Galápagos region is ideally suited to address this objective. As an intermediate spreading center (40-65 mm/yr), the axial topography of the GSC should be particularly sensitive to small changes in spreading rate or magma supply. Magma supply is also expected to vary systematically along the GSC with increasing distance from the Galápagos hotspot allowing the effect of this variable to be studied largely independent of spreading rate changes. We will show that the GSC, like the SEIR, is characterized by three distinct axial morphologies: an axial high, an axial valley, and a distinctive transitional axial morphology (TAM) consisting of a broad region, up to 20 km wide, of rough volcanic and fault-generated topography. We also find that the transition from axial high to rift valley along the GSC occurs over a distance of ~200-300 km along-axis and is accompanied by gravity-estimated crustal thickness variations of >1-2 km; while the change from axial high to TAM is produced in less than 9 km. Bathymetric roughness of the ridge flanks increases as ridge morphology evolves from axial high to TAM to rift valley. Analysis of on- and off-axis depth variations suggests that ~15-40% of the axial topography is dynamically supported.

2. Tectonic Setting

The GSC lies in the eastern Pacific, about 170 km north of the Galápagos Archipelago, and represents the tectonic boundary between the Cocos and Nazca plates (Figure 1). The GSC is an intermediate-rate spreading center, with full spreading rates increasing from ~40 mm/yr in the west to ~65 mm/yr in the east [*DeMets et al.*, 1994]. The eastern portion of the GSC is offset by several large transform faults, most notably the Panamá Fracture Zone (FZ) at 83°W, the Ecuador FZ at 84.5°W, and the Inca FZ at 85.5°W (Figure 2). Between 85.5°W and its triple junction with the EPR at 102°W, the GSC is offset by only one major transform at 91°W, also known as the Galápagos FZ (Figure 2). The complicated tectonic evolution of the GSC during the last 8 Myr has been extensively studied by *Wilson and Hey* [1995]. The kinematic history of the GSC west of 85°W has been dominated by rift propagation, mainly away from the Galápagos

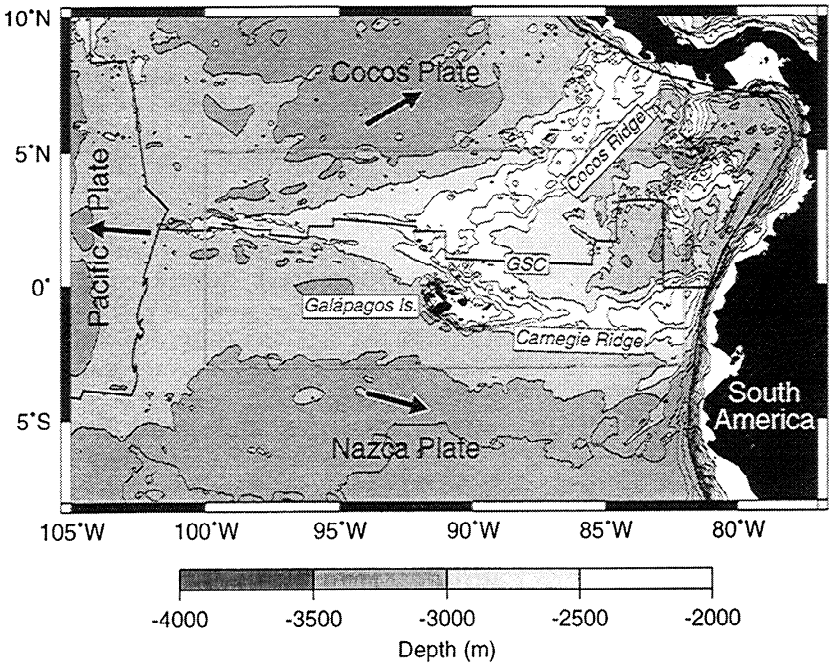

Figure 1. Bathymetry map of the eastern equatorial Pacific showing the Cocos and Nazca plates and the east-west trending Galápagos Spreading Center (GSC). Contours every 500 m. The plate motion relative to a hotspot reference frame is indicated by the arrows [*Gripp and Gordon,* 1990]. Box indicates the location of Figure 2 and the Galápagos'96 survey reported in this paper.

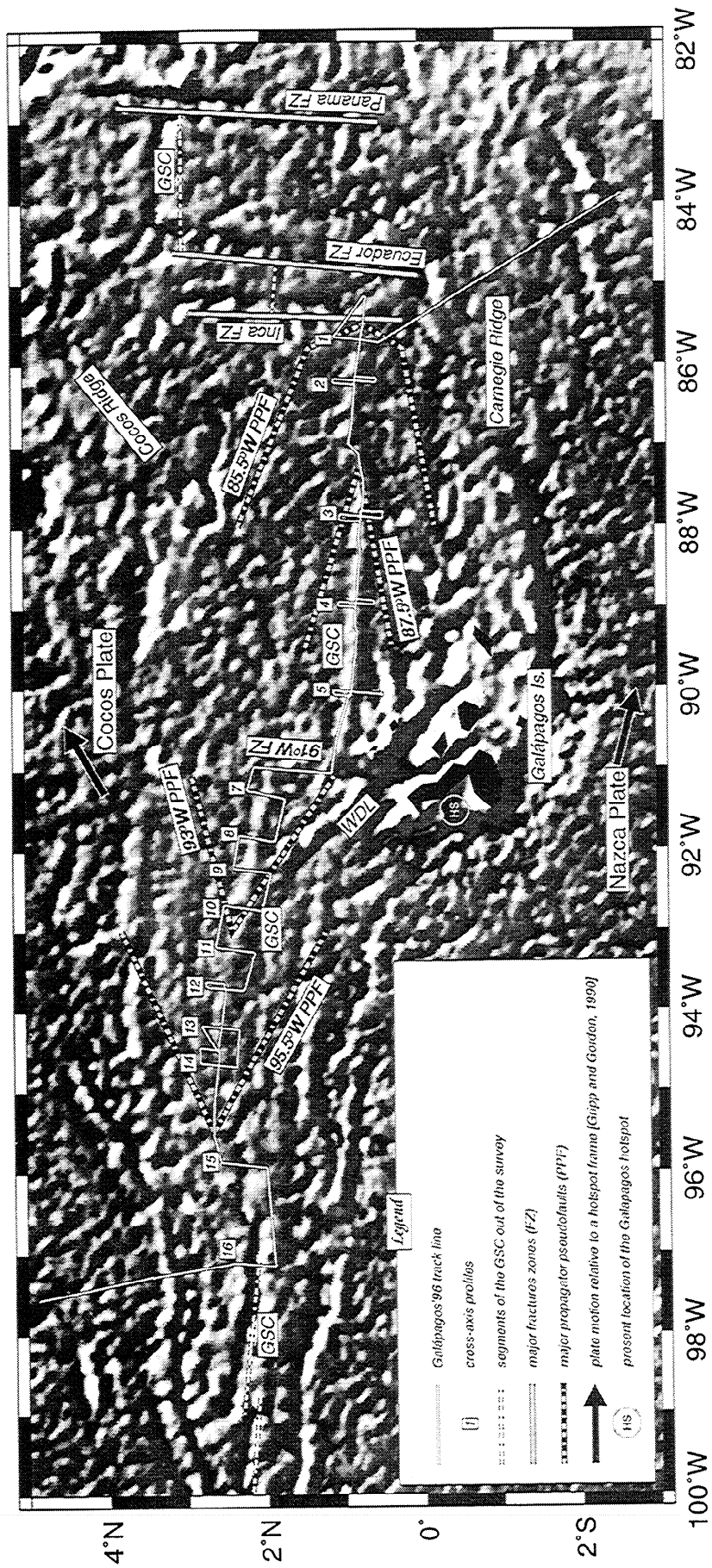

Figure 2. Satellite gravity relief of the Galápagos Spreading Center (GSC) [*Sandwell and Smith*, 1994] illuminated from the NE. Galápagos'96 navigation track is denoted by the white line. Major tectonic features are marked (see legend). WDL corresponds to the Wolf-Darwin Lineament.

hotspot, and ridge jumps predominately to the south forming new spreading segments near the hotspot. During this period of time, the GSC has experienced three major changes in spreading rate at 1.5, 4.1, and 5.2 Myr [*Wilson and Hey*, 1995]. Major propagating ridge tips/overlapping spreading centers (OSC) are currently located along the GSC at 95.5°W and 93°W west of the hotspot, and at 87.5°W and 85.5°W east of it (Figure 2).

The GSC is a classic example of an oceanic ridge influenced by a nearby hotspot [*Vogt*, 1976; *Morgan*, 1978], and a convenient natural laboratory within which to study the effect of magma supply on axial morphology. The Galápagos hotspot activity may have started ~80-90 Myr ago [*Richards et al.*, 1991]. The hotspot was located on the GSC from ~25 Ma until 10 Ma, forming the Cocos and Carnegie ridges (Figure 1) [*Hey*, 1977]. Over the last 10 Myr, the GSC has migrated northward with respect to the hotspot, and the Galápagos Archipelago began its formation on the Nazca plate. The Galápagos hotspot is presently located ~170 km south of the GSC, beneath Isla Fernandina (Figure 2) [*Graham et al.*, 1993; *Sinton et al.*, 1996].

The influence of the Galápagos hotspot on the GSC has been observed in both geophysical and geochemical studies. The spreading center sits atop a regional bathymetric swell that extends ~1300 km along the Cocos-Nazca plate boundary. The ridge axis shallows by ~1100 m along the Galápagos swell reaching a minimum depth of ~1750 m at the intersection with the 91°W FZ (Figure 1) [e.g., *Hey*, 1977; *Allmendinger and Riis*, 1979; *Ito and Lin*, 1995]. The Galápagos swell is associated with a -90 mGal mantle Bouguer anomaly which also reaches a minimum near 91°W [*Ito and Lin*, 1995]. These variations in depth and gravity have been explained by crustal thickening of up to 4 km and a gradual increase in mantle temperature of 50 ± 25 °C beneath the ridge axis toward the point on the ridge closest to the hotspot (91°W FZ) [*Ito and Lin*, 1995]. *Schilling et al.* [1982] and *Verma et al.* [1983] have reported anomalous rare earth element and isotope ratios along the GSC. The maximum anomaly is found near 92°W, with a gradual decrease to the east and west along the GSC away from that point. These observations are explained by the entrainment of plume material to the GSC and its dispersal along the ridge axis [*Vogt*, 1976; *Schilling et al.*, 1982; *Verma and Schilling*, 1982]. The flow pattern of mantle material from the hotspot is uncertain, but probably occurs through a sublithospheric conduit or prevailing structure as *Morgan* [1978] and *Schilling et al.* [1982] suggested. The geochemical anomaly peak at ~92°W [*Verma and Schilling*, 1982; *Verma et al.*, 1983], as well as the proximity between the southern edge of the 91°W FZ and the present location of the hotspot, supports the hypothesis that such transform offset is a preferred structure along which the plume material reaches the GSC. We thus use the 91°W FZ as our reference origin to investigate morphological variations along the GSC.

3. Data

This study is based on new data acquired in April 1996 on board the Spanish research vessel B/O *Hespérides* during the Galápagos'96 experiment [*Dañobeitia et al.*, 1996]. The data set includes Simrad EM12 multibeam bathymetry, seafloor backscatter, and magnetics. The experiment was designed to acquire geophysical observations along the GSC, from 85°W to 97°W. In addition, several across-axis swaths were surveyed in order to obtain detailed information on the ridge axis and the young adjacent seafloor (<1 Ma) in ~50 km long across-axis profiles. For technical reasons, swath bathymetry is only available between ~85°W and 90°W (profiles 1-5) and between ~93.5°W and 95°W (profiles 12-14) (Figure 2).

In this paper we analyze the variation in axial morphology along the GSC using multibeam bathymetry data collected along and across the ridge axis. Figure 3 shows a compilation of 15 cross-axis profiles arranged from east (top) to west (bottom) plotted as a function of spreading rate. The present location of the ridge axis is obtained from bathymetric and magnetic profiles. Magnetic anomalies were obtained by removing the 1995 International Geomagnetic Reference Field from the observed values. They were inverted with the bathymetry profiles to obtain magnetization profiles. The inversion has been performed using the method of *Parker and Huestis* [1974], assuming a 0.5 km thick magnetized layer. In all of the profiles, there is a clear central magnetization peak which allows accurate location of the neovolcanic zone. Where a distinct axial high or valley is observed, the magnetization high correlates with topography. In areas where the topography is transitional between an axial high and a valley, the ridge axis cannot be easily identified from bathymetry, and the central magnetization high is used to locate the axis.

Spreading rates were calculated using the Euler vector from *DeMets et al.* [1994]. Axial depth for each of the 15 profiles was measured by averaging the depth in a 4 km wide across-axis bin centered on the ridge axis. Off-axis depth is measured at 10 km north and south of the ridge axis, averaging data within a 2 km wide window. The difference between off-axis depth calculated north and south of the ridge is negligible (<100 m) and lies within the error estimation. Thus hereafter references to off-axis depth implies measurements south of the ridge. To estimate seafloor roughness, we selected northern and southern segments of each across-axis profile that were longer than 15 km after excluding their central zone to avoid influence of ridge morphology. Roughness was then calculated as the standard deviation of depth along the segment after removing a linear trend.

4. Results

The GSC is marked by systematic, along-axis changes in ridge morphology between the Inca FZ at 85°W and the 95.5°W propagator (Figure 3). The portion of the GSC nearest the Galápagos hotspot, both east and west of the 91°W FZ, is associated with an EPR-like axial high (profiles 4-10). This axial high is taller (~400-700 m) and broader (~20 km across at its base) than typical cross-sections of the EPR (Figure 4a) and has a cross-sectional area nearly 2 times the mean value of the EPR [*Scheirer and Macdonald*, 1993]. West of 92°W, the axial high develops a distinctive summit rift or graben ~30-50 m deep and ~1-2 km wide (profiles 9 and 10). Farther from the 91°W FZ, the axial high broadens and deepens, eventually forming a TAM that is neither an axial high or an axial valley (profiles 11-14 west of the Galápagos FZ and profiles 1-3 east of the FZ). The boundary between the TAM and the axial high found along the GSC nearest the hotspot approximately coincides with the 93°W propagator/OSC on the west and is located near 88.5°W on the east (Figure 2). West of 95°W the ridge axis develops a distinct axial valley (profiles 15 and 16). On profile 15 this rift valley is about 20 km wide and 400 m deep, with a central volcanic ridge ~5 km wide and ~300 m high located on the valley floor. At 97°W the ridge axis is marked by a 1500 m deep rift valley with dimensions comparable to the rift valleys found along the slow spreading MAR (Figure 4b). Thus along this one plate boundary

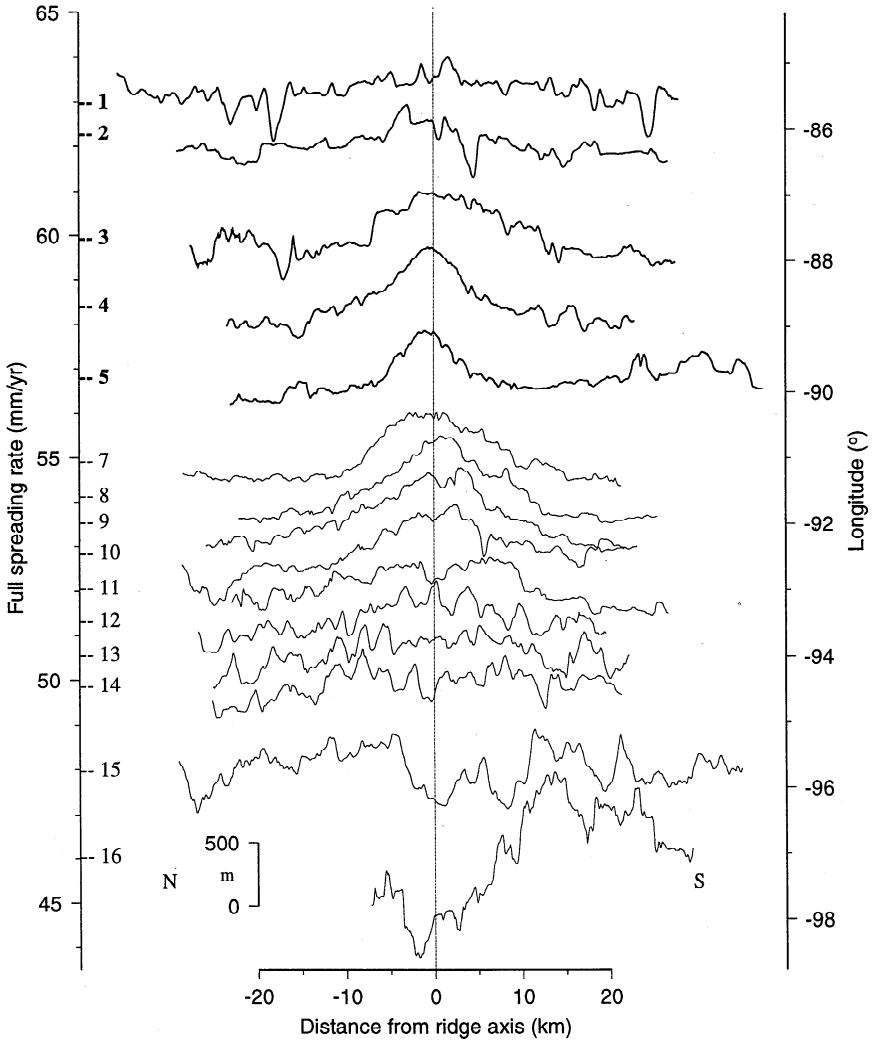

Figure 3. Center beam bathymetry profiles across the GSC. Profile locations shown in Figure 2. Scales to the left and right of the profiles show the full spreading rate and longitude for each profile. Profiles east of the 91°W FZ are represented by thick lines, while profiles west of the 91°W FZ are plotted as thin lines. Note that the portion of the GSC nearest the Galápagos hotspot (between 87.5°W and 93°W, profiles 4-10) is associated with an EPR-like axial high, while at increasing distance from the hotspot the axial high disappears (profiles 1-3 and 11-14) eventually forming a rift valley (profiles 15 and 16). These variations in axial morphology are largely independent of variations in spreading rate.

between 91°W and 97°W, with spreading rates varying only between 55 and 46 mm/yr, we see the entire range of ridge axis morphology observed along the global mid-ocean ridge system.

4.1. Transitional Axial Morphology (TAM)

Significant sections of the GSC are associated with an unusual TAM that is neither an axial high or a rift valley. This intermediate morphology is present along a nearly 200 km long section of the GSC between 93°W and 95°W and along 200-300 km between 88°W and the Inca FZ at 85.5°W. Figure 5 and Plate 1 show several examples of the TAM. Within this transitional region the axial topography can be highly variable along-axis and asymmetric in cross section. It often consists of a broad region, up to 20 km across, of very rough terrain consisting of short linear features, sometimes with an axial graben (Figures 5a and 5d and Plates 1b and 1c), fault-bounded highs elevated above the surrounding seafloor (Figure 5b and Plate 1a), or broad swells upon which ~100-200 m high, ~5 km wide ridges have developed (Figure 5c and 5d and Plate 1c). Small axial volcanoes up to 200 m high sometimes occur within the axial zone (Plate 1c). With this complex topography the ridge axis is difficult to identify. However, a distinct magnetization high is usually present over the neovolcanic zone (Figure 5). The width of this magnetization high is comparable to that observed along other sections of the GSC suggesting the presence of a relatively distinct, narrow neovolcanic zone despite the complex topographic expression of the ridge axis. The maximum reflectivity along the backscatter profiles coincides with the magnetization high over the neovolcanic zone (Figure 5), constraining the ridge axis identification. However, the extension of the accretionary zone cannot be inferred from the backscatter intensity, which it is controlled by both young volcanism and topographic relief.

Change from TAM to axial high east of the 91°W FZ occurs between profile 3 (~88°W) and profile 4 (~89°W). The detailed

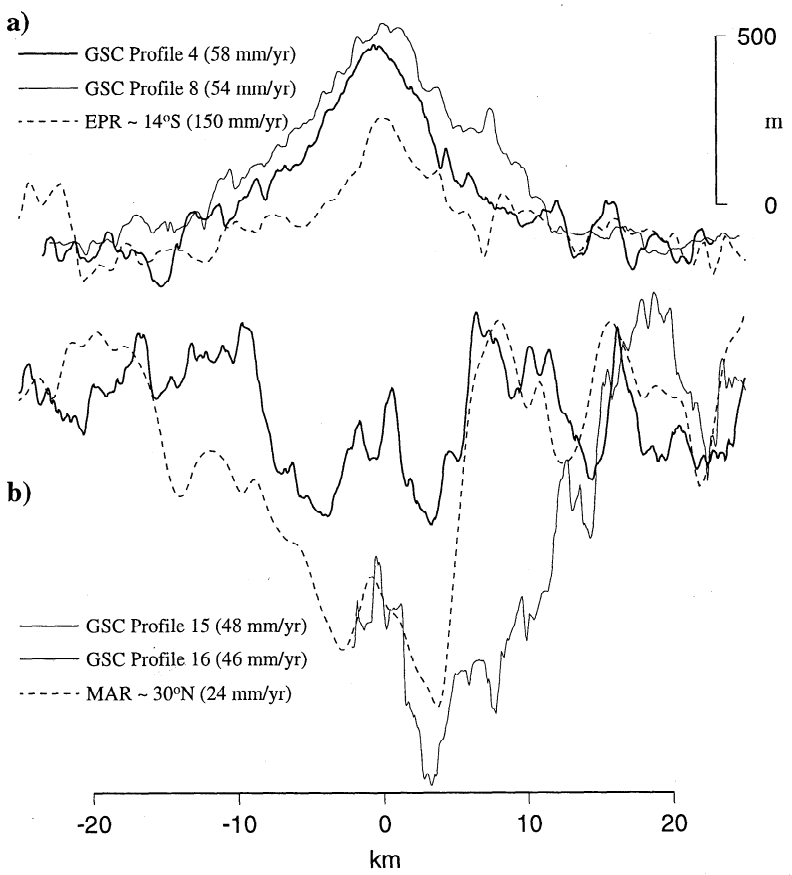

Figure 4. (a) Comparison of GSC axial highs (thin line, profile 8; thick line, profile 4) with across-axis profile of EPR at 14°S (dashed line). Note that the axial high at the GSC is wider and higher than at the EPR. (b) Comparison of GSC axial valleys (thin line, profile 16; thick line, profile 15) with across-axis profile of MAR at 30°N (dashed line). Near 97°W the GSC has a MAR-like rift valley. Full spreading rates are indicated in parentheses.

analysis of the multibeam bathymetry acquired along-axis between those profiles constrains the scale of such transition. Figure 6 shows the topographic expression of the GSC between 88°22'-88°50'W. Axial high morphology is well developed west of 88°37'W, while east of 88°32'W TAM is observed. The change from TAM to axial high then occurs over a distance of about 9 km, which we consider an abrupt morphological change.

4.2. On- and Off-Axis Depth Variations and Flank Roughness

In Figure 7 the changes in on- and off-axis depth and flank roughness are referenced to distance to the 91°W FZ, our reference frame for evaluating the influence of the hotspot on axial morphology. At increasing distance from the 91°W FZ, axial depth increases by 1600 m toward the west and by ~800 m toward the east (Figure 7a). Axial highs are observed at water depths of 1700-2100 m, and the TAM is associated with depths of 2100-2750 m, while rift valleys are present at depths of 2900-3300 m. Off-axis depths also increase with distance from the 91°W FZ (Figure 7b). However, this increase is much smaller than observed along-axis, and is about 600 m both east and west of the 91°W FZ.

Assuming that the off-axis depth variation is entirely due to changes in crustal thickness and mantle temperature, then the difference between the on- and off-axis depth variation can be interpreted in terms of dynamic topography. We excluded profiles 15-16 from this analysis since the deepening of the valley floor and shoaling of the rift flanks may have a non isostatic origin [*Chen and Morgan*, 1990]. However, axial highs and TAM profiles probably do not have a significant component of dynamic topography off-axis and are associated with ~565-695 m of off-axis depth variations. Hence excluding the rift valley, changes in crustal thickness and mantle temperature are probably responsible for the 60-85% of the ~820-950 m of axial depth variation observed along the GSC, with the remaining 15-40% due to dynamically supported topography.

Seafloor roughness increases with distance to the 91°W FZ and hence as morphology evolves from axial high to TAM to rift valley (Figure 7c). Although there are only two measurements of roughness at axial highs and three at axial valleys, the pattern observed in Figure 7c follows the general relationship between seafloor roughness and axial morphology/spreading rate described from different mid-ocean ridges [*Goff*, 1992; *Goff et al.*, 1993, 1997; *Ma and Cochran*, 1997; *Small and Sandwell*, 1992; *Small*, 1994]. Axial highs are associated with roughness values of 30-70 m, TAM are associated with 30-90 m, and axial valleys are associated with 80-110 m.

4.3. Morphological and Bathymetric Asymmetry Along the GSC

While axial morphology varies systematically along the GSC with increasing distance from the 91°W FZ, these changes are not symmetric about the FZ. Cross-axis profiles at equal distances

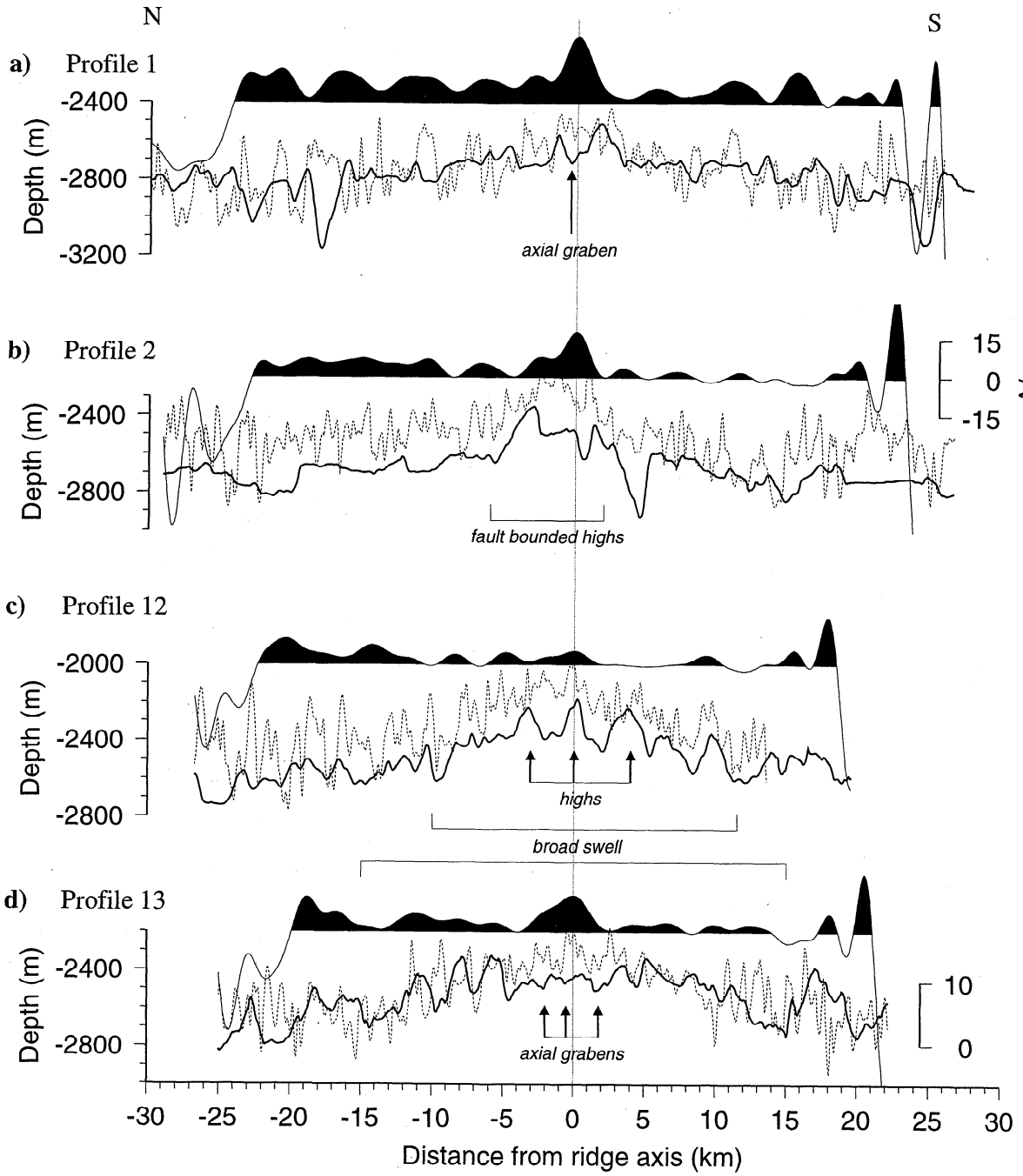

Figure 5. Selected bathymetry profiles across the ridge axis illustrating the transitional axial morphology observed along the GSC. Thin lines represent across-axis bathymetry, dotted lines are seafloor backscatter, and solid areas represent positive crustal magnetization: (a) profile 1, (b) profile 2, (c) profile 12, and (d) profile 13. See Figure 2 for location. Note variable character of this transitional morphology which is neither an axial high or a rift valley. Scales at the right of Figures 5b and 5d correspond to magnetization and backscatter (normalized reflectivity of the seafloor), respectively.

from the 91°W FZ are compared in Figure 8. Profile 11, ~250 km west of the 91°W FZ, has a transitional morphology, while at a comparable distance east of the FZ, profile 4 has a distinct axial high. West of 94°W (~550 km from the 91°W FZ) a rift valley is clearly developed (profiles 15 and 16), while as far east as the Inca FZ at 85.5°W (~600 km from the 91°W FZ), the ridge crest topography is still transitional (profiles 1 and 2).

This asymmetry is also reflected in axial depths which are ~500 m shallower east of the 91°W FZ than at comparable distances west of the FZ (Figure 7a). The shallowest portion of the GSC is centered near the 91°W FZ (our reference point). However, axial depth variations along the GSC are symmetric about a point located ~100 km east of the FZ, as observed in Figure 7a. This could be interpreted as an spreading rate effect, or

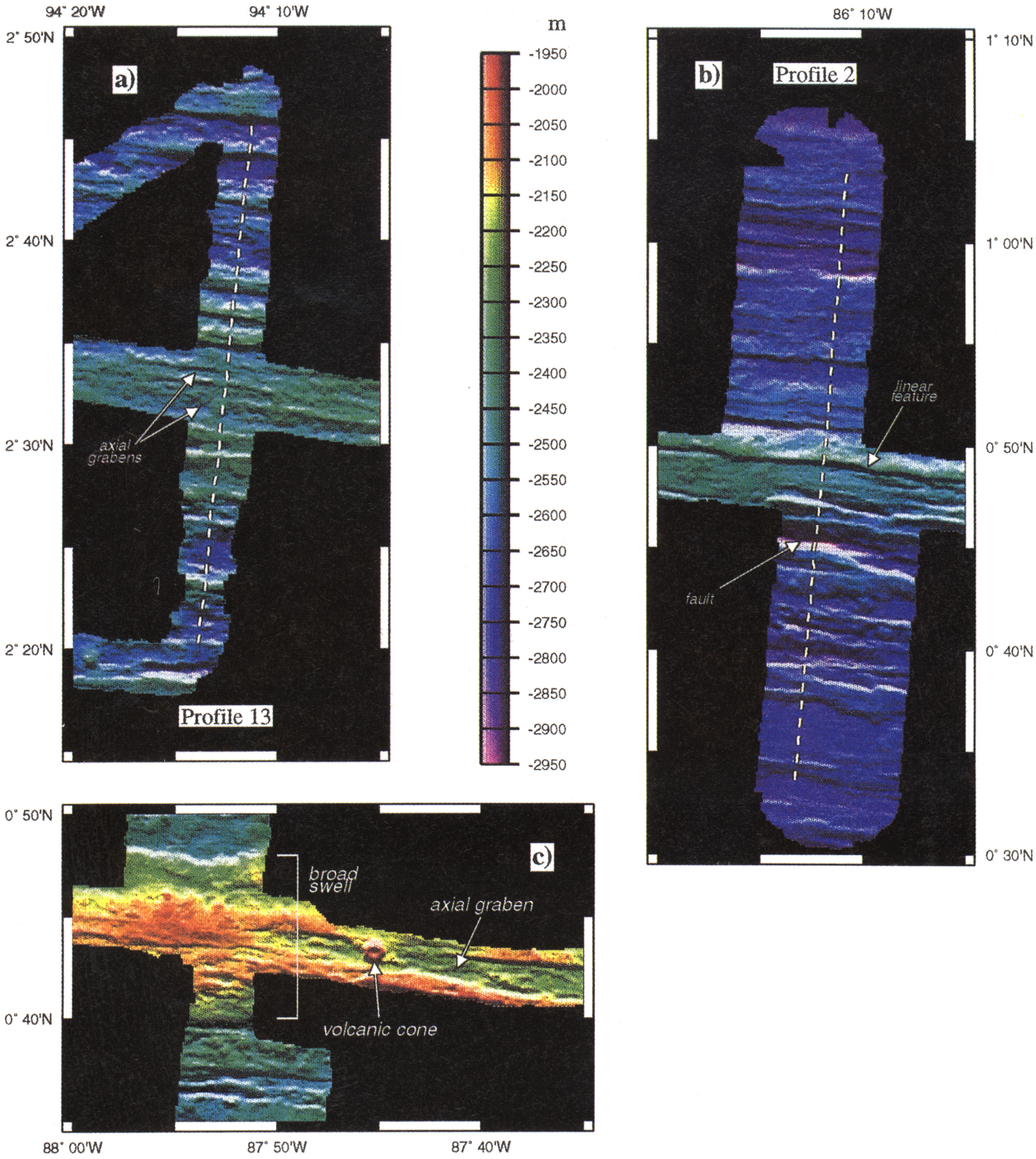

Plate 1. Color shaded topography for three representative examples of transitional axial topography along the GSC. (a) Cross-axis profile 2, (b) cross-axis profile 13, and (c) along-axis bathymetry near profile 3. See Figure 2 for location. Dashed white lines in Plates 1a and 1b mark location of profile. Note the variable character of this transitional topography, with both volcanic constructional features (e.g. the axial seamount near 87°45'W in Plate 1c), fault-bounded linear features (Plate 1a), and axial grabens (Plate 1b).

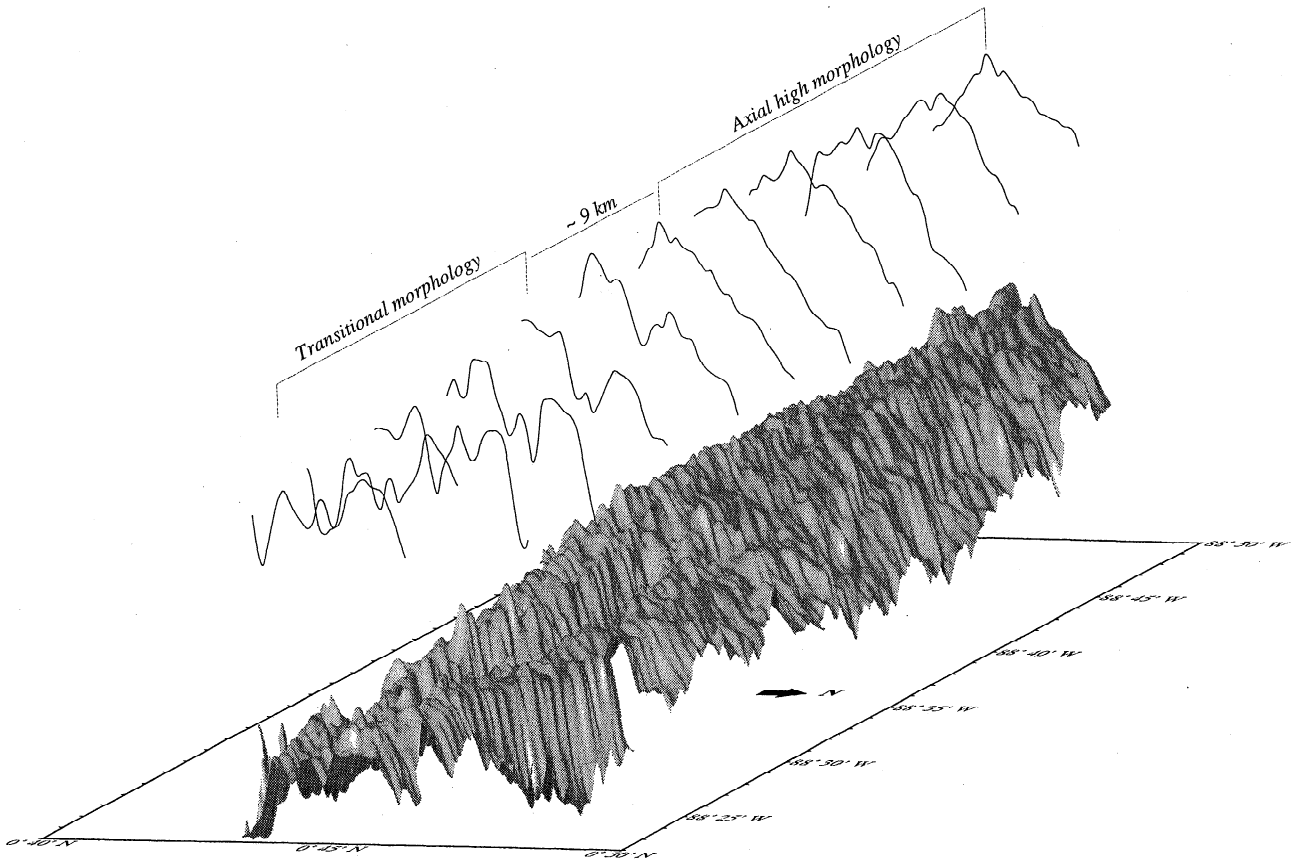

Figure 6. Shaded relief of the GSC between 88°22'W and 88°50'W. Solid lines are bathymetric cross sections every 4.5 km. Note the rapid transition (~9 km) from an axial high to the transitional morphology.

a preferred eastward flow of plume material, or both. The existence of a distinct, symmetric geochemical anomaly centered at ~92°W [*Verma et al.*, 1983] does not support the possibility of an asymmetry in plume material flow along the GSC and thus favors a spreading rate control for the asymmetry in both axial depth and morphology. The asymmetry observed in the on-axis depth is not reflected in the off-axis depth variations (Figure 7b). This observation also supports the idea that crustal thickness variations are symmetric about the 91°W FZ and again favors the hypothesis that increasing spreading rate from west to east primarily controls the morphological, and hence the bathymetric, asymmetry observed along the GSC.

5. Discussion

5.1. Changes in Axial Morphology

Sempéré et al. [1997] and *Ma and Cochran* [1996] describe two types of morphology along the SEIR which are not either EPR- or MAR-like and define them as "rifted axial high" and "shallow axial valley." SEIR-rifted axial highs are characterized by a broad, low 150-250 m relief high with a 50-200 m deep summit depression on top of it, and SEIR shallow axial valleys by a 10-15 km wide valley with 100-500 m relief. Comparison of such morphologies with the transitional one presented in this paper shows that the SEIR-rifted axial high and GSC-TAM are equivalent morphologies. Transitions between the three types of morphologies observed at the SEIR (MAR-like, shallow rift valley, and axial high) are well-defined and occur over short lengths of the ridge axis. Along the GSC we find a well-defined transition between axial high and TAM, while the transition from TAM to rift valley cannot be constrained from our data. The rapid variation from TAM to an axial high shown in Figure 6 supports the idea that abrupt and large changes in axial yield strength primarily control the axial morphology, but in a two-step threshold phenomenon rather than in a single-step as predicted by *Phipps Morgan and Chen* [1993].

Morphological transitions along the SEIR are accompanied by abrupt changes in roughness, except for the EPR-like to rifted axial high transition [*Ma and Cochran*, 1997; *Goff et al.*, 1997]. Similarly, Figure 7c shows that morphological variations along the GSC are associated with changes in seafloor roughness. The mean roughness for each of the morphologies is 55±25 m (highs), 65±20 m (TAM), and 100±15 m (valleys). These values, with their large uncertainty, are lower than those estimated at the SEIR for the equivalent morphologies [*Goff et al.*, 1997]. However, they support the hypothesis that ridge flank roughness is sensitive to axial morphology and thus can be used as an indicator of paleochanges in spreading rate and/or magma supply.

As noted by *Ma and Cochran* [1996], the existence of a distinct transitional morphology suggests that more than one threshold mechanism might be operative. They speculate that the change from rift valley to transitional may be controlled by the development of a ductile lower crust as proposed by *Chen and Morgan* [1990], while the change from transitional to axial high may mark the development of a steady state crustal magma chamber as proposed by *Phipps Morgan and Chen* [1993]. The

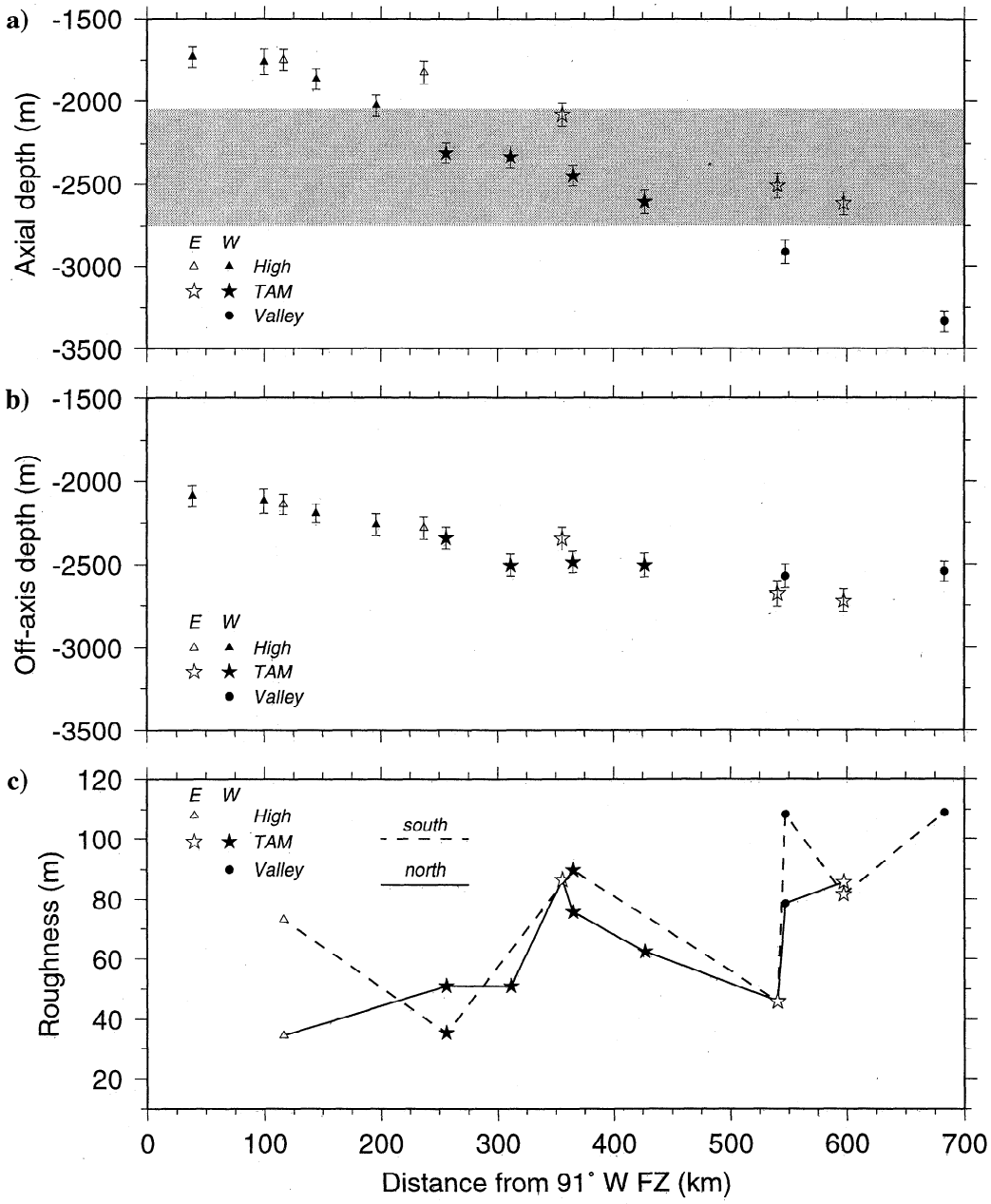

Figure 7. (a) Axial depths of each across-axis profile plotted versus distance from the 91°W FZ. Axial depths are calculated by averaging the depth in 4 km wide bins centered on the ridge. Error bars represent the standard deviation. Solid symbols represent profiles west of the 91°W FZ, and open symbols represent profiles east of the 91°W FZ. Triangles denote axial highs, stars denote transitional morphology and circles denote axial valleys. Shaded gray zone highlights the range of depths associated with each morphological type. (b) Off-axis depth calculated by averaging the depth in 4 km wide bins centered 10 km south of the ridge axis. (c) Estimated roughness of the across-axis profiles plotted versus distance from the 91°W FZ. Note the increasing roughness as the morphology changes from axial high to transitional and axial valley.

acquisition of multichannel reflection data along the GSC across these morphological transitions would provide a good test of these hypotheses.

5.2. Axial Morphology and Crustal Thickness Variations

The observations described in section 4 are consistent with the hypothesis that the increased magma supply associated with the Galápagos hotspot is primarily responsible for the systematic variations in axial morphology observed along more than 1300 km of the GSC between 85°W and 97°W. In Figure 9b we show how the morphological variations observed along the GSC correlate with *Ito and Lin's* [1995] predicted crustal thickness variation along the GSC. Figure 9 suggests that an increase in crustal thickness of >1-2 km accompanies the transition from a rift valley to an axial high in this area. However, the differences in the along-axis and off-axis depth variations displayed in Figures 7a and 7b suggest a dynamic origin for some of the along-axis depth variation. *Ito and Lin* [1995] propose that along-axis mantle Bouguer and bathymetry anomalies are supported by a crustal thickening of ~3 km from the distal ends

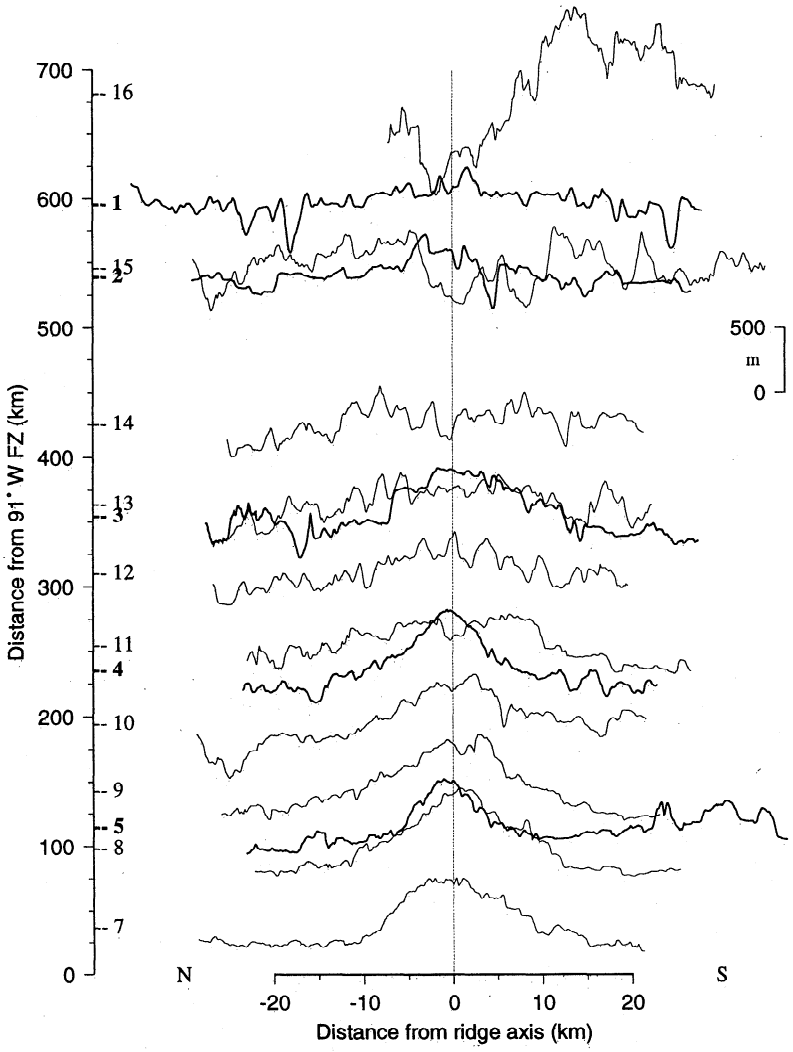

Figure 8. Center beam bathymetry profiles across the GSC. Scale to the left of the profiles shows the distance from the 91°W FZ for each profile. Profiles east of the 91°W FZ are represented by thick lines, while thin lines are the profiles east of the 91°W FZ. Note the different axial morphologies east and west of the 91°W FZ at similar distances. For example, ~540 km from the FZ the ridge is characterized by an axial valley to the west (profile 15) and by a transitional morphology at the east (profile 2). At ~250 km from the FZ, an axial high is observed at the east (profile 4) and transitional morphology is observed to the west (profile 11).

of the ridge toward the 91°W FZ (75% of the anomalies) and a mantle temperature increase of 50±25°C (25% of the anomalies). They claim that their results are upper bounds of crustal thickening and mantle temperature: if processes such as melt depletion, buoyancy-driven mantle flow, and mantle compositional effects on melting and mantle densities are considered, lower values of mantle temperature and crustal thickening would be predicted. Comparison of axial and off-axis bathymetry (Figures 7a and 7b) support Ito and Lin's prediction that crustal thickening and mantle temperature changes along the GSC are probably lower than 3 km and 50°C, respectively.

A crustal thickening related to the transition from rift valley to an axial high is consistent with the dependence of ridge axis morphology on magma supply and spreading rate predicted by *Phipps Morgan and Chen* [1993], namely, that at full spreading rates of 50-60 mm/yr the transition from rift valley to axial high should occur at a crustal thickness of about 6-7 km (assuming Nu=12; see Figure 10). The relationship between axial morphology, spreading rate, and predicted crustal thickness along the GSC is compared with Phipps Morgan and Chen model in Figure 10. Axial valleys at the GSC fall where the transition from axial valley to high is predicted, while TAM and axial highs are observed where the model predicts axial highs (existence of magma lens). This could be interpreted as indicating that TAM is associated with a crustal magma chamber, though perhaps one which is smaller or shorter lived than those associated with axial highs. However, *Ito and Lin* [1995] predict crustal thickness variations but not absolute crustal thickness. If the crust along the GSC is ~2 km thinner than they have assumed, then axial valleys would correlate with the absence of a magma lens and axial highs with the presence of such structures, and TAM would fall in the transition of both cases, depending on model parameters (Figure 10). Hence the existence or the absence of magma chambers at mid-ocean ridges where TAM is observed, as well as the knowledge of crustal thickness, is a crucial input that should be incorporated in future models of ridge-axis morphology and crustal accretion.

The *Phipps Morgan and Chen* [1993] model also predicts a

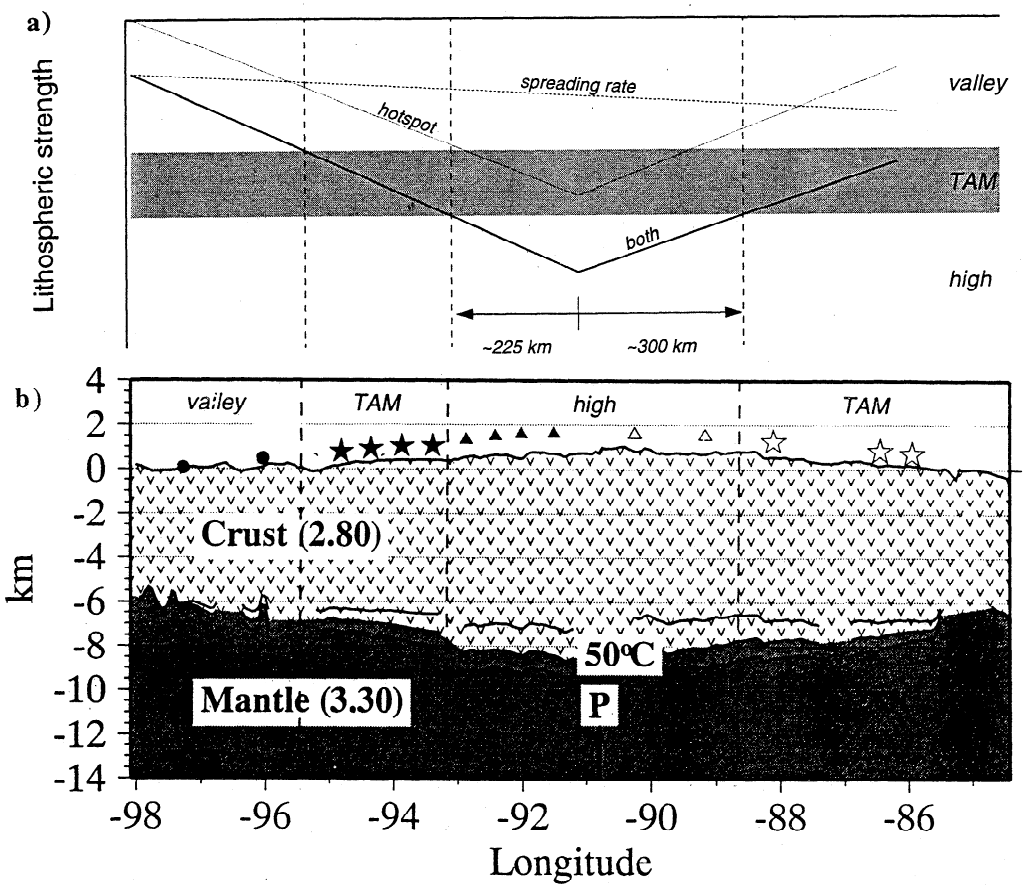

Figure 9. (a) Schematic cartoon showing the combined (solid line) effects of spreading rate (dashed line) and hotspot magma supply (dotted line) on axial lithospheric strength responsible of asymmetric variations in axial morphology along the GSC. (b) Relationship between axial morphology and crustal thickness variations along the GSC. Crustal thicknesses are from *Ito and Lin* [1995]; symbols are as in Figure 6. The transition from axial high to rift valley morphology along the GSC is not abrupt but occurs over a distance of 200-300 km along-axis and is accompanied by gravity-estimated crustal thickness variations of >1-2 km. (Modified after *Ito and Lin* [1995]; 50°C denotes their best fitting thermal model, and P locates the 91°W FZ.)

much sharper threshold in axial morphology than we observe at the GSC. In their ridge crest thermal model at full spreading rates of 60 mm/yr, a crustal thickness variation of <0.5 km results in a large change in the depth of the 1200°C isotherm and in axial yield strength (see Figure 2 of *Phipps Morgan and Chen* [1993]). Instead, we find a more gradual transition from rift valley to axial high that is associated with >1-2 km of crustal thickening and a distinctive, transitional ridge axis morphology which is not predicted by this model.

5.3. Along-Axis Asymmetry With Respect to the Hotspot

An interesting result of this study is the distinct asymmetry in the morphological and axial depth variations along the GSC observed across the 91°W FZ. As noted earlier, the axial high topography found along the GSC near the hotspot extends farther east of the 91°W FZ than to the west, and the rift valley which develops west of 94°W is not found at comparable distances along the GSC east of the 91°W FZ (Figure 8). This asymmetry could be the result of the increase in spreading rate along the GSC from 46 mm/yr at 97°W to 63 mm/yr at 85.5°W (Figure 3). Axial thermal structure is a function of both spreading rate and crustal thickness. At faster spreading rates the transition from an axial high to a rift valley is expected to occur at a smaller crustal thickness [*Phipps Morgan and Chen*, 1993] (see Figure 10). Assuming the variation in crustal thickness is approximately symmetric about the 91°W FZ (see Figure 9), then the variations in axial morphology should occur on thinner crust (i.e., farther from the hotspot) east of the 91°W FZ because of the faster spreading rates there. Thus the asymmetry in morphological changes along the GSC may reflect the combined effects of mantle temperature (controlled by plume entrainment and dispersal along the ridge axis) and spreading rate (magma delivered to the crust per unit time) on axial thermal structure and morphology. A simplified cartoon explaining the morphological asymmetry in terms of the lithospheric strength is presented in Figure 9a. As spreading rate increases, lithosphere becomes weaker (dashed lines). Moreover, the higher magma supply from the Galápagos hotspot, which we assume to be symmetric about the 91°W FZ, also decreases lithospheric strength (dotted line). The combination of both processes produces an asymmetric variation of lithospheric strength from the 91°W FZ (solid line). Consequently, changes in axial morphology are observed closer to the FZ to the west rather than to the east.

Figure 7a shows that axial depths are ~500 m shallower at comparable distances east of the 91°W FZ than to the west. This suggests that mantle temperatures may also be higher and/or crustal thickness may be greater along the GSC east of the

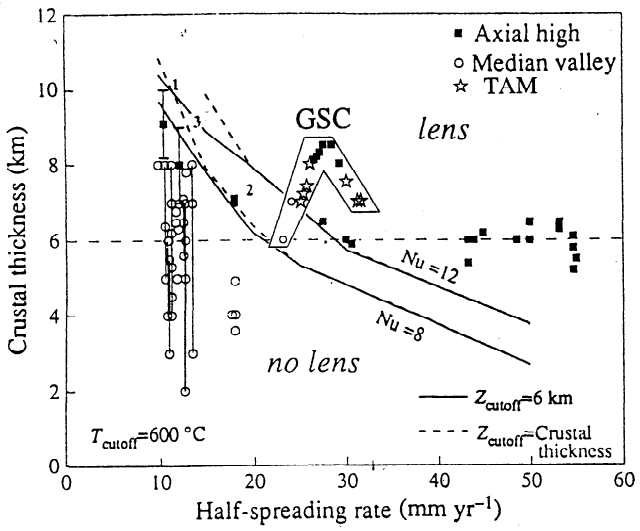

Figure 10. Comparison of relationship between axial morphology, spreading rate, and crustal thickness along the GSC with predictions of *Phipps Morgan and Chen* [1993] model. See text for discussion. (Modified after *Phipps Morgan and Chen* [1993]. Note that half spreading rate values are used, while in the text full spreading rates values are always used. *Nu* is the Nusselt number, or ratio of hydrothermal heat transport to heat transport by heat conduction. Z_{cutoff} is the maximum depth of hydrothermal penetration. T_{cutoff} is the hydrothermal temperature limit over which rocks are impermeable.)

hotspot. However, this hypothesis is not confirmed by the off-axis depth variations. The absence of any asymmetry across the 91°W FZ in off-axis depth (Figure 7b) excludes the possibility of an asymmetry in crustal thickness and/or mantle temperature from the FZ as the origin of the axial depth asymmetry. Moreover, as pointed out previously, the geochemical anomaly peak at 92°W [*Verma et al.*, 1983] suggests a more robust magma supply westward of the 91°W FZ than eastward. Thus the smoother eastward deepening of ridge-axis could be interpreted in terms of the global relationship between axial depth and spreading rate, since axial depth decreases with spreading rate for full rates less than 80 mm/yr [e.g., *Small*, 1994].

Thus the existence of axial high morphology along the GSC between ~88.5°W and 92.5°W, and the bathymetric swell centered in the 91°W FZ can be attributed to an increase in magma supply from the Galápagos hotspot, while the asymmetry in morphological and axial depth variations reflects a spreading rate control.

6. Conclusions

1. The GSC is marked by systematic, along-axis changes in axial morphology between the Inca FZ at 85°W and the 95.5°W propagator. The portion of the GSC nearest the Galápagos hotspot, both east and west of the Galápagos FZ at 91°W, is associated with an EPR-like axial high. At increasing distance from the hotspot the axial high broadens and deepens, forming a distinctive transitional morphology consisting of a broad region, up to 20 km wide, of very rough volcanic and fault-generated topography. West of the 94°W, the ridge axis develops a rift valley typical of the slow spreading MAR.

2. These systematic changes in axial morphology are primarily caused by variations in magma supply and crustal thickness along the GSC due to the entrainment and dispersal of hot, plume mantle from the nearby Galápagos hotspot.

3. There is not an abrupt change from axial high to rift valley along the GSC, but a distinct TAM occurs over a distance of ~200-300 km along-axis and is accompanied by gravity-estimated crustal thickness variations of >1-2 km. The boundary between axial high and this TAM is quite abrupt. This morphological change occurs along a segment less than 9 km long.

4. Along-axis depth variations are larger than off-axis variations, indicating that 15-40% of the axial bathymetry is dynamically supported.

5. Seafloor roughness at the flanks of the GSC supports the hypothesis that roughness is primarily controlled by axial morphology.

6. Morphological and axial depth variations along the GSC are asymmetric respect to the 91°W FZ. We attribute this to a spreading rate control.

Aknowledgments. We thank Captain Francisco Lara Arias and the crew of the B/O *Hespérides* for their assistance during the Galápagos'96 experiment and Ecuador authorities who gave us all kinds of facilities to work within the exclusive economic zone of Galápagos Archipelago. We also thank JGR reviewers Garret Ito and Christopher Small and Associate Editor John Goff for their helpful suggestions and constructive criticism. The GMT software package [*Wessel and Smith*, 1995] was used in the preparation of this paper. Galápagos'96 experiment was supported by CICYT project ANT94-0182-C02-02. Additional funding was provided by CIRIT (project #1995SGR00438). First author J.P.C. was granted by MEC scholarship PN93-28992999. R.S.D. and E.E.E.H. were supported by NSF (OCE-9402033).

References

Allmendinger, R.W., and F. Riis, The Galápagos rift at 86°W, 1, Regional morphological and structural analysis, *J. Geophys. Res., 84*, 5379-5389, 1979.

Chen, Y., and W. J. Morgan, Rift valley/no rift valley transition at mid-ocean ridges, *J. Geophys. Res., 95*, 17,571-17,581, 1990.

Cochran, J.R., J.-C. Sempéré, and SEIR Scientific Team, The Southeast Indian Ridge between 88°E and 118°E: gravity anomalies and crustal accretion at intermediate spreading rates, *J. Geophys. Res., 102*, 15,463-15,487, 1997.

Dañobeitia, J.J., R.S. Detrick, M. Farrán, D. Naar, and the Galápagos'96 Working Group, Geophysical investigation of ridge-hotspot interaction at the Galápagos Spreading Center, *InterRidge News, 5*(2), 32-35, 1996.

DeMets, C., R. G. Gordon, D. F. Argus, and S. Stein, Effect of recent revisions to the geomagnetic reversal time scale on estimates of current plate motions, *Geophys. Res. Lett., 21*, 2191-2194, 1994.

Goff, J.A., Quantitative characterization of abyssal hill morphology along flow lines in the Atlantic Ocean, *J. Geophys. Res., 97*, 9183-9202, 1992.

Goff, J.A., A. Malinverno, D.J. Fornari, and J.R. Cochran, Abyssal hill segmentation: quantitative analysis of the East Pacific Rise flanks 7°S-9°S, *J. Geophys. Res., 98*, 13,851-13,862, 1993.

Goff, J.A., Y. Ma, A. Shah, J.R. Cochran, and J.-C. Sempéré, Stochastic analysis of seafloor morphology on the flank of the Southeast Indian Ridge: The influence of ridge morphology on the formation of abyssal hills, *J. Geophys. Res., 102*, 15,521-15,534, 1997.

Gràcia, E., C. Tisseau, M. Maia, T. Tonnerre, J.-M. Auzende, and Y. Lagabrielle, Variability of the axial morphology and of the gravity structure along the Central Spreading Ridge (North Fiji Basin): Evidence for contrasting thermal regimes, *Mar. Geophys. Res., 18*, 249-273, 1996.

Graham, D. W., D. M. Christie, K. S. Harpp, and J. E. Lupton, Mantle plume helium in submarine basalts from the Galápagos Platform, *Science, 262*, 2023-2026, 1993.

Gripp, A. E., and R. G. Gordon, Current plate velocities relative to the hotspots incorporating the NUVEL-1 global plate motion model, *Geophys. Res. Lett., 17*, 1109-1112, 1990.

Hey, R., Tectonic evolution of the Cocos-Nazca spreading center, *Geol. Soc. Am. Bull.*, *88*, 1404-1420, 1977.

Hooft, E.E.E., and R.S. Detrick, Relationship between axial morphology, crustal thickness, and mantle temperature along the Juan de Fuca and Gorda Ridges, *J. Geophys. Res.*, *100*, 22,499-22,508, 1995.

Ito, G., and J. Lin, Mantle temperature anomalies along the present and paleoaxes of the Galápagos spreading center as inferred from gravity analyses, *J. Geophys. Res.*, *100*, 3733-3745, 1995.

Ma, Y., and J.R. Cochran, Transitions in axial morphology along the Southeast Indian Ridge, *J. Geophys. Res.*, *101*, 15,849-15,866, 1996.

Ma, Y., and J.R. Cochran, Bathymetric roughness of the Southeast Indian Ridge: Implications for crustal accretion at intermediate spreading rate mid-ocean ridge, *J. Geophys. Res., 102,* 17,697-17,711, 1997.

Macdonald, K. C., Mid-ocean ridges: Fine scale tectonic, volcanic and hydrothermal processes within the plate boundary zone, *Annu. Rev. Earth Planet. Sci., 10,* 155-190, 1982.

Morgan, W. J., Rodríguez, Darwin, Amsterdam,..., A second type of hotspot island, *J. Geophys. Res.*, *83*, 5355-5360, 1978.

Parker, R. L., and S. P. Huestis, The inversion of magnctic anomalics in the presence of topography, *J. Geophys. Res.*, *79*, 1587-1593, 1974.

Phipps Morgan, J., and Y. J. Chen, Dependence of ridge-axis morphology on magma supply and spreading rate, *Nature*, *364*, 706-708, 1993.

Richards, M. A., D. L. Jones, R. A. Duncan, and D. J. DePaolo, A mantle plume initiation model for the Wrangellia flood basalt and other oceanic plateaus, *Science*, *254*, 263-267, 1991.

Sandwell, D. T., and W. H. F. Smith, New global marine gravity grid based on stacked ERS-1, Geosat and Topex altimetry, *Eos Trans. AGU 75*(16) Spring Meet. Suppl., 321, 1994.

Scheirer, D. S., and K. C. Macdonald, Variation in cross-sectional area of the axial ridge along the East Pacific Rise: Evidence for magmatic budget of a fast spreading center, *J. Geophys. Res.*, *98*, 7871-7885, 1993.

Schilling, J.-G., R. H. Kingsley, and J. D. Devine, Galápagos hot spot-spreading center system, 1, Spatial petrological and geochemical variations (85°W-101°W), *J. Geophys. Res.*, *87*, 5593-5610, 1982.

Searle, R. C., and A. S. Laughton, Fine scale sonar study of tectonics and volcanism on the Reykjanes Ridge, *Oceanol. Acta*, *4*, 5-18, 1981.

Sempéré, J-C., J. Palmer, D. M. Christie, J. Phipps Morgan, and A. N. Shor, Australian-Antarctic Discordance, *Geology*, *19*, 429-432, 1991.

Sempéré, J-C., J.R. Cochran, and SEIR Scientific Team, The Southeast Indian Ridge between 88°E and 120°E: variations in crustal accretion at constant spreading rates *J. Geophys. Res., 102,* 15,489-15,505, 1997.

Sinton, C. W., D. M. Christie, and R. Duncan, Geochronology of Galápagos seamounts, *J. Geophys. Res.*, *101*, 13,689-13,700, 1996.

Small, C., A global analysis of mid-ocean ridge axial topography, *Geophys. J. Int., 116,* 64-84, 1994.

Small, C., and D. T. Sandwell, An abrupt change in ridge axis gravity with spreading rate, *J. Geophys. Res.*, *94*, 17,383-17,392, 1989.

Small, C., and D. T. Sandwell, An analysis of ridge axis gravity roughness and spreading rate, *J. Geophys. Res.*, *97*, 3235-3245, 1992.

Verma, S. P., and J.-G. Schilling, Galápagos hot spot-spreading center system, 2, $^{87}Sr/^{86}Sr$ and large ion lithophile element variations (85°W-101°W), *J. Geophys. Res.*, *87*, 10,838-10,856, 1982.

Verma, S. P., J.-G. Schilling, and D. G. Waggoner, Neodymium isotopic evidence for Galápagos hotspot-spreading center evolution, *Nature*, *306*, 654-657, 1983.

Vogt, P. R., Plumes, subaxial pipe flow and topography along the mid-ocean ridge, *Earth Planet. Sci. Lett.*, *29*, 309-325, 1976.

Wessel, P., and W.H.F. Smith, New version of the generic mapping tools released, *Eos Trans. AGU, 76,* 329, 1995.

Wilson, D. S., and R. Hey, History of rift propagation and magnetization intensity for the Cocos-Nazca spreading center, *J. Geophys. Res.*, *100*, 10,041-10,056, 1995.

R. Bartolomé and J. J. Dañobeitia, Departamento de Geofísica, Instituto de Ciencias de al Tierra (Consejo Superior de Investigaciones Científicas), Lluís Solé i Sabarís s/n, 08028 Barcelona, Spain.

J. P. Canales, R. S. Detrick, and E. E. E. Hooft, Department of Geology and Geophysics, Woods Hole Oceanographic Institution, 360 Woods Hole Road, Woods Hole, MA 02543. (e-mail: juan@sienna.whoi.edu)

D. F. Naar, Department of Marine Sciences, University of South Florida, St. Petersburg, FL 33701.

(Received January 8, 1997; revised May 15, 1997;
accepted June 4, 1997.)